A multi-material HLLC Riemann solver with both elastic and plastic waves for 1D elastic-plastic flows

Li Liu[1],Junbo Cheng [1,*], Jiequan Li [1]

January 12, 2019

Abstract

A multi-material HLLC-type approximate Riemann solver with both the elastic and plastic waves (MHLLCEP) is constructed for 1D elastic-plastic flows with a hypo-elastic constitutive model and the von Mises yielding condition. Comparing with the HLLCE Riemann solver introduced in Cheng, during constructing MHLLCEP, we do not use any assumption and so describe and evaluate the plastic waves more accurate than that in HLLCE. Moreover, if the non-linear waves in the Riemann problem are only shock waves, even with the plastic waves, MHLLCEP is theoretically accurate. For multi-material system, in this paper, a ghost cell method is also used to achieve a high-order spatial reconstruction across the interface without oscillation. Based on MHLLCEP, combining with the third-order WENO reconstruction method and the third-order Runge-Kutta method in time, a high-order cell-centered Lagrangian scheme for 1D multi-material elastic-plastic flows is built in this paper. A number of numerical experiments are carried out and numerical results showed the presented third-order scheme is convergent, stable, and essentially non-oscillatory. Moreover, for multi-material elastic-plastic flows, the scheme with MHLLCEP is more accurate and more reasonable in resolving the multi-material interface than the scheme with HLLCE.

1 Introduction

In this paper, a multi-material elastic-plastic HLLC-type approximate Riemann solver(MHLLCEP) is developed, with the capability of resolving both elastic and plastic waves, to simulate one-dimensional multi-material elastic-plastic solid problems with the isotropic elastic-plastic model [1] and von Mises' yielding condition in the framework of high-order cell-centered Lagrangian scheme.

Generally, elastic-plastic flows can be mainly simulated in three ways, Eulerian method [2, 3, 4], staggered Lagrangian schemes [1] and cell-centered Lagrangian schemes [5, 6, 7, 8] which is considered in this paper. Cell-centered Lagrangian scheme is derived based on the Godunov methods and has combined many advantages from both staggered Lagrangian schemes and Eulerian methods. Firstly, it's no necessary to use artificial viscosity which always is used in the staggered Lagrangian schemes; Secondly, it is easy to guarantee the total energy conservation; Besides, it can also be used to simulate the problems with both hyper-elastic and hypo-elastic models [5, 6, 7, 8] as a Lagrangian scheme.

In the Godunov-type method, a core process is to construct the conservative flux by solving a Riemann problem at each cell face. As the Riemann problem contains many physical structures, especially in elastic-plastic flows, such as elastic waves, plastic waves and contact waves or interfaces between different materials, the property of the approximate Riemann solver may do a magnitude influence in the simulation. Recently, there is a lot of works have been done in this area. For example, Gavrilyuk et al. [9] analyzed the structure of Riemann solution to construct a Riemann solver for the linear elastic system of hyperbolic non-conservative models for transverse waves, wherein an extra evolution equation was added in order to make the elastic transformations reversible in the absence of shock wave. Despres [10] built a shock solution to a non-conservations reversible system of hypo-elasticity models and found that a sonic point is necessary to construct compression solution that begins at a constrained compressed state. Cheng eta al. [11] analyzed the wave structures of one-dimensional elastic-plastic flows and developed an effective two-rarefaction approximate Riemann solver with elastic waves (TRRSE) and build the second-order and third-order cell-centered Lagrangian schemes

based on the TRRSE, but the TRRSE is a little expensive as iteration method is used in it. In [12], for one-dimensional elastic-plastic flows, Cheng introduced a HLLCE Riemann solver, which is fast and efficient in resolving elastic waves and plastic waves for numerical examples in [12], but Cheng evaluated the deviatoric stresses from the following *assumption: a pressure is continuous across the contact wave* in the Riemann solver. This assumption is valid for pure fluids, but for elastic-plastic flows, this assumption may lead to some errors. There are three cases we need to consider.

1. If both states in the star regions between the contact wave are elastic, this assumption does not results in errors;
2. If the both states reach the elastic limit, there are two cases we need take into account:
   (a) if both the materials across the interface are same, this assumption does not results in errors, too;
   (b) if both the materials are different, this assumption will result in big errors because the yielding strengths of different materials are different;
3. If one state in one side of the interface are yielded, but another does not, this assumption also results in big errors.

For the above consideration, in this paper, we aim to construct a new HLLC-type Riemann solver which is suitable for 1D multi-material elastic-plastic flows. In the new solver, both the elastic waves and plastic waves are resolved and the assumption in [12] that the pressure is continuous across the interface is deleted; Correspondingly, the errors introduced by the assumption will also be eliminated.

With a high-order reconstruction method, one stencil may across the interface and in a multi-material state, which will cause oscillation near the interface. In this paper, we use a ghost cell method in multi-material system to obtain a stable high-order reconstruction. Combined with an improved third-order WENO scheme[13] and Runge-Kutta scheme, a high-order cell-centered Lagrangian scheme is given in this paper for one-dimensional multi-material elastic-plastic flows.

This paper is organized as follows. In section 2, we briefly introduce the governing equations to be studied. In section 3, the MHLLEP method is constructed. Then, high-order elastic-plastic cell-centered Lagrangian scheme is given in section 4. Some numerical examples are presented to validate the method. Conclusions are shown in section 5.

2 Governing equations

The equations for a continuous one-dimensional solid in differential form are given as

$$\partial_t \mathbf{U} + \partial_x \boldsymbol{F}(\mathbf{U}) = 0,\ x \in\ \Omega \subset \mathbf{R},\ t > 0,$$

where

$$\mathbf{U} = \begin{bmatrix} \rho \\ \rho u \\ \rho E \end{bmatrix}, \quad \mathbf{F} = \begin{bmatrix} \rho u \\ \rho u^2 - \sigma_x \\ (\rho E - \sigma_x) u \end{bmatrix}, \tag{2.1}$$

ρ, u, σ_x and E are the density, velocity in $x-$direction, Cauchy stress and total energy per unit volume, respectively, E has the relation with specific internal energy e as

$$E = e + \frac{1}{2}u^2, \tag{2.2}$$

$$\sigma_x = -p + s_{xx}, \tag{2.3}$$

where p and s_{xx} denote hydrostatic pressure and deviatoric stress in the $x-$ direction, respectively.

In this paper, the elastic energy is not included in the total energy. The exclution of the elastic energy is usual for practical engineering problems [7] and is different from that in Ref.[9].

The relation of the pressure with the density and the specific internal energy is gotten from the equation of state (EOS). In this paper, we consider the Mie-Grüneisen EOS,

$$p(\rho, e) = \rho_0 a_0^2 f(\eta) + \rho_0 \Gamma_0 e, \tag{2.4}$$

where $f(\eta) = \frac{(\eta-1)(\eta-\Gamma_0(\eta-1)/2)}{(\eta-s(\eta-1))^2}$, $\eta = \frac{\rho}{\rho_0}$, ρ_0, a_0, s, and Γ_0 are constant parameters of the Mie-Grüneisen EOS.

Hooke's law is used here to describe the relationship between the deviatoric stress and the strain,

$$\dot{s}_{xx} = 2\mu \left(\dot{\varepsilon}_x - \frac{1}{3}\frac{\dot{V}}{V} \right), \tag{2.5}$$

where μ is the shear modulus, V is the volume, and the dot means the material time derivative,

$$\dot{()} = \frac{\partial()}{\partial t} + u\frac{\partial()}{\partial t}, \tag{2.6}$$

and

$$\dot{\varepsilon}_x = \frac{\partial u}{\partial x}, \quad \frac{\dot{V}}{V} = \frac{\partial u}{\partial x}. \tag{2.7}$$

By using Eq.(2.7), Eq.(2.5) can be rewritten as

$$\frac{\partial s_{xx}}{\partial t} + u\frac{\partial s_{xx}}{\partial t} = \frac{4}{3}\mu\frac{\partial u}{\partial x}. \tag{2.8}$$

The Von Mises' yielding condition is used here to describe the elastic limit. In one spatial dimension, the von Mises' yielding criterion is given by

$$|s_{xx}| \leq \frac{2}{3}Y_0, \tag{2.9}$$

where Y_0 is the yield strength of the material in simple tension.

3 MHLLCEP

3.1 The Riemann problem

The Riemann problem for the 1D time dependent elastic-plastic equations is given as follows:

$$\begin{cases} \partial_t \rho + \partial_x(\rho u) = 0, \\ \partial_t(\rho u) + \partial_x(\rho u^2 + p - s_{xx}) = 0, \\ \partial_t(\rho E) + \partial_x\left[(\rho E + p - s_{xx})u\right] = 0, \\ \partial_t s_{xx} + u\partial_x s_{xx} - \frac{4}{3}\partial_x u = 0, \\ |s_{xx}| \leq \frac{2}{3}Y_0, \\ Q(x, t=0) = \begin{cases} Q_L, \text{ if } x < 0, \\ Q_R, \text{ if } x \geq 0, \end{cases} \end{cases} \tag{3.1}$$

where $Q = (\rho, \rho u, \rho E, s_{xx})^T$.

3.2 Jacobian matrix

For the Mie-Grüneisen EOS, the system (3.1) can be written as

$$\partial_t \boldsymbol{Q} + \boldsymbol{J}(\boldsymbol{Q})\partial_x \boldsymbol{Q} = 0, \tag{3.2}$$

where

$$J=\begin{bmatrix} 0 & 1 & 0 & 0 \\ -u^2+\frac{\partial p}{\partial \rho}+\Gamma(\frac{u^2}{2}-e) & u(2-\Gamma) & \Gamma & -1 \\ (\Gamma(\frac{u^2}{2}-e)-e+\frac{\sigma_x}{\rho}+\frac{\partial p}{\partial \rho})u & -\Gamma u^2-\frac{\sigma_x}{\rho}+e & (1+\Gamma)u & -u \\ \frac{4}{3}\mu\frac{u}{\rho} & -\frac{4}{3}\mu\frac{1}{\rho} & 0 & u \end{bmatrix}, \tag{3.3}$$

where $\Gamma=\frac{\Gamma_0\rho_0}{\rho}$.

The eigenvalues of the coefficient matrix $\boldsymbol{J}(\boldsymbol{Q})$ are given as

$$\lambda_1=\lambda_2=u, \quad \lambda_3=u-c, \quad \lambda_4=u+c, \tag{3.4}$$

where

$$\begin{cases} c=\sqrt{a^2-\dfrac{\rho_0}{\rho^2}\Gamma_0 s_{xx}+\dfrac{4}{3}\dfrac{\mu}{\rho}}, \\ a^2=\dfrac{\partial p}{\partial \rho}+\dfrac{p}{\rho^2}\dfrac{\partial p}{\partial e}=a_0^2\dfrac{\partial f}{\partial \eta}+\dfrac{p}{\rho^2}\rho_0\Gamma_0. \end{cases} \tag{3.5}$$

The corresponding right eigenvectors are

$$r_1=\begin{bmatrix} \frac{1}{b_1} \\ \frac{u}{b_1} \\ 0 \\ 1 \end{bmatrix}, \quad r_2=\begin{bmatrix} -\frac{\Gamma}{b_1} \\ -\frac{\Gamma u}{b_1} \\ 1 \\ 0 \end{bmatrix}, \quad r_3=\frac{1}{\phi^2}\begin{bmatrix} 1 \\ u-c \\ h-uc \\ \phi^2 \end{bmatrix}, \quad r_4=\frac{1}{\phi^2}\begin{bmatrix} 1 \\ u+c \\ h+uc \\ \phi^2 \end{bmatrix}, \tag{3.6}$$

where

$$b_1=\frac{\partial p}{\partial \rho}-\Gamma E, \quad h=E+\frac{p-s_{xx}}{\rho}, \tag{3.7}$$

and

$$\phi^2=a^2-\frac{\rho_0}{\rho^2}\Gamma_0 s_{xx}-c^2=-\frac{4\mu}{3}\frac{1}{\rho}. \tag{3.8}$$

3.3 Formulations between the contact wave or the interface

For a system without molecular diffusion, there is no materials convecting cross the contact wave or interface, so the velocities between the discontinuity are always equal, $u_L^*=u_R^*$. This can also be verified by the eigenvectors in Eq.(3.6).

Using the eigenvectors in Eq.(3.6), for the λ_1-wave we have

$$\frac{d\rho}{\frac{1}{b_1}}=\frac{d\rho u}{\frac{u}{b_1}}=\frac{d\rho E}{0}=\frac{ds_{xx}}{1}. \tag{3.9}$$

From the above equations, we can easily deduce that

$$du=0, \quad d(s_{xx}-p)=0, \tag{3.10}$$

which means

$$u_L^*=u_R^*, \tag{3.11}$$

and

$$\sigma_{x,L}^*=\sigma_{x,R}^*, \tag{3.12}$$

where $()_L^*$ and $()_R^*$ denote $()$ in the region of $\mathbf{W}_L^*$ and $\mathbf{W}_R^*$, respectively. Here we do not show the details of the derivation for simplicity of presentation.

Using the eigenvectors (3.6), for the λ_2-wave we have

$$\frac{d\rho}{\frac{-\Gamma}{b_1}}=\frac{d\rho u}{\frac{-u\Gamma}{b_1}}=\frac{d\rho E}{1}=\frac{ds_{xx}}{0}. \tag{3.13}$$

From the above equations, we can easily deduce that

$$du = 0, \quad dp = 0, \quad ds_{xx} = 0, \tag{3.14}$$

which means

$$u_L^* = u_R^*, \tag{3.15}$$

$$p_L^* = p_R^*, \quad s_{xx,L}^* = s_{xx,R}^*, \tag{3.16}$$

where $()_L^*$ and $()_R^*$ denote () in the region of $\mathbf{W}_L^*$ and $\mathbf{W}_R^*$, respectively.

From Eq.(3.16), we get that

$$\sigma_{x,L}^* = \sigma_{x,R}^*. \tag{3.17}$$

At last, for the λ_1 and λ_2 waves, one can find that the following two equations always hold:

$$u_L^* = u_R^*, \quad \sigma_{x,L}^* = \sigma_{x,R}^*. \tag{3.18}$$

Using the Rankine-Hugoniot relations between the contact wave or the interface

$$\boldsymbol{F}_R^* = \boldsymbol{F}_L^* + s^*(\boldsymbol{U}_R^* - \boldsymbol{U}_L^*), \tag{3.19}$$

where s^* denotes the velocity of the contact wave.

From the first and second components of the above system, one can get

$$\rho_R^* u_R^* = \rho_L^* u_L^* + s^*(\rho_R^* - \rho_L^*), \tag{3.20}$$

$$\rho_R^* u_R^{*2} - \sigma_R^* = \rho_L^* u_L^{*2} - \sigma_L^* + s^*(\rho_R^* u_R^* - \rho_L^* u_L^*). \tag{3.21}$$

Generally, for convenience, we define

$$s^* = u_L^* = u_R^*. \tag{3.22}$$

3.4 A relation between ρ and s_{xx} in 1D elastic-plastic equation system

According to (2.6), from the 1D elastic-plastic equations in Eq.(3.1), the equations of the density and the deviatoric stress can be written as

$$\frac{\partial u}{\partial x} = -\frac{1}{\rho}\frac{d\rho}{dt}, \tag{3.23}$$

and

$$\frac{ds_{xx}}{dt} = \frac{4}{3}\mu\frac{\partial u}{\partial x}. \tag{3.24}$$

Substituting (3.23) into (3.24) yields

$$\frac{ds_{xx}}{dt} = -\frac{4}{3}\mu\frac{1}{\rho}\frac{d\rho}{dt}. \tag{3.25}$$

Take an integration,

$$s_{xx1} = -\frac{4}{3}\mu\ln(\frac{\rho_1}{\rho_0}) + s_{xx0}. \tag{3.26}$$

The subscripts 1 and 0 mean the states in front of and behind a wave, respectively. This relation always holds if there is no yielding in the integration path.

3.5 Building MHLLCEP

Now we considered the constructing details of MHLLCEP. As left-going or right-going plastic waves exist possibly, there may be three to five waves in the Riemann structure, which depends on the yielding state on the left side and right side of the interface.

3.5.1 Pre-evaluating the states without considering of plastic waves

At first we do not know whether the states in the star region around the contact wave reach the elastic limit or not, so firstly *assume that there is no plastic wave in and the material is totally yielding or totally not yielding* (**Assumption** 1). Based on **Assumption** 1, using the HLLC method, we can get the states in the star regions of the Riemann structure showed in Fig.1. If the obtained state contains yielding process, we will consider the cases showed in Fig.2-4.

The Riemann structure of MHLLCEP in Fig.1 is given as follows,

$$\boldsymbol{U}_{\text{Case1}}^{\text{MHLLCEP}}(x,t)=\begin{cases}\boldsymbol{U}_L, & \text{if} \quad \dfrac{x}{t}\le s_L,\\ \boldsymbol{U}_L^*, & \text{if} \quad s_L\le\dfrac{x}{t}\le s^*,\\ \boldsymbol{U}_R^*, & \text{if} \quad s^*\le\dfrac{x}{t}\le s_R,\\ \boldsymbol{U}_R, & \text{if} \quad \dfrac{x}{t}\ge s_R,\end{cases} \tag{3.27}$$

and the corresponding Eulerian numerical flux and Lagrangian numerical flux are

$$\boldsymbol{F}_{\text{Case1}}^{\text{Euler}}(x,t)=\begin{cases}\boldsymbol{F}_L, & \text{if} \quad \dfrac{x}{t}\le s_L,\\ \boldsymbol{F}_L^*, & \text{if} \quad s_L\le\dfrac{x}{t}\le s^*,\\ \boldsymbol{F}_R^*, & \text{if} \quad s^*\le\dfrac{x}{t}\le s_R,\\ \boldsymbol{F}_R, & \text{if} \quad \dfrac{x}{t}\ge s_R,\end{cases} \tag{3.28}$$

$$\boldsymbol{F}_{\text{Case1}}^{\text{Lag}}(x,t)=\begin{cases}\boldsymbol{f}_L^*, & \text{if} \quad s_*\ge\dfrac{x}{t},\\ \boldsymbol{f}_R^*, & \text{if} \quad s^*\le\dfrac{x}{t},\end{cases} \tag{3.29}$$

where s^* denotes the speed of the contact wave, $f=(0,p-s_{xx},(p-s_{xx})u)^T$.

According to the Rankine-Hugoniot conditions between left elastic wave, one can get

$$\boldsymbol{F}_L^*=\boldsymbol{F}_L+s_L(\boldsymbol{U}_L^*-\boldsymbol{U}_L). \tag{3.30}$$

The first and second components of the above system can be written as

$$\rho_L^*u_L^*=\rho_Lu_L+s_L(\rho_L^*-\rho_L), \tag{3.31}$$

and

$$\rho_L^*u_R^{*2}-\sigma_L^*=\rho_Lu_L^2-\sigma_L+s_L(\rho_L^*u_L^*-\rho_Lu_L). \tag{3.32}$$

Using the relation of $u_L^*=u_R^*=s^*$ in Eq.(3.22), the speed of contact wave can be evaluated as

$$\hat{s}^*=\frac{\sigma_L-\sigma_R+\rho_Lu_L(s_L-u_L)-\rho_Ru_R(s_R-u_R)}{\rho_L(s_L-u_L)-\rho_R(s_R-u_R)}, \tag{3.33}$$

the density is solved as

$$\hat{\rho}_L^*=\frac{\rho_L(u_L-s_L)}{\hat{s}^*-s_L}. \tag{3.34}$$

Similarly, the density behind the right elastic wave is

$$\hat{\rho}_R^*=\frac{\rho_R(u_R-s_R)}{\hat{s}^*-s_R}. \tag{3.35}$$

According to Eq.(3.26), the deviatoric stress is evaluated as

$$\hat{s}_{xxL}^*=-\frac{4}{3}\mu\ln(\frac{\hat{\rho}_L^*}{\rho_L})+s_{xxL},\quad \hat{s}_{xxR}^*=-\frac{4}{3}\mu\ln(\frac{\hat{\rho}_R^*}{\rho_R})+s_{xxR}. \tag{3.36}$$

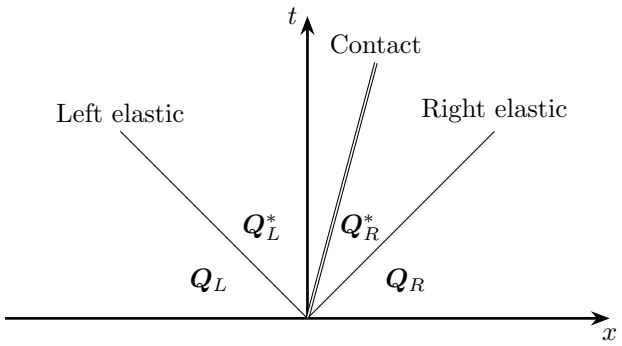

Figure 1: The structures of MHLLCEP method, case 1: without plastic wave.

If the speeds of left and right elastic waves are given, we can evaluate all states in the star region between the contact wave. Here we define the speeds of left and right elastic waves as

$$s_L = \min(u_L - c_L, u_R - c_R, 0), \quad s_R = \max(u_L + c_L, u_R + c_R, 0). \tag{3.37}$$

Using the pre-evaluated values of $\hat{s}^*_{xxL}$ and $\hat{s}^*_{xxR}$ in (3.36), we can classify the true condition into the following four cases.

3.5.2 Case 1: No plastic wave

If $|s_{xxL}| < \frac{2}{3}Y_0$ and $|\hat{s}^*_{xxL}| < \frac{2}{3}Y_0$, all the states in the left are not yielding and there is no plastic wave; similarly, If $|s_{xxL}| \geq \frac{2}{3}Y_0$ and $|\hat{s}^*_{xxL}| \geq \frac{2}{3}Y_0$, all the states in the left are yielding, there is also plastic wave. All the same things happen in the right. In this case, the structures of the Riemann solver are showed in Fig.1.

Then

$$s^* = \hat{s}^*, \quad \rho^*_L = \hat{\rho}^*_L, \quad \rho^*_R = \hat{\rho}^*_R, \tag{3.38}$$

$$s^*_{xxL} = \Upsilon(\hat{s}^*_{xxL}), \quad s^*_{xxR} = \Upsilon(\hat{s}^*_{xxR}) \tag{3.39}$$

where,

$$\Upsilon(\omega) = \begin{cases} \omega, \text{ if } |\omega| \leq \dfrac{2}{3}Y_0, \\ \dfrac{2}{3}Y_0, \text{ if } \omega > \dfrac{2}{3}Y_0, \\ -\dfrac{2}{3}Y_0, \text{ if } \omega < -\dfrac{2}{3}Y_0. \end{cases} \tag{3.40}$$

The Cauchy stresses are solved by Eq.(3.32),

$$\sigma^*_L = \sigma^*_R = \sigma_L - \rho_L(s_L - u_L)(s^* - u_L).$$

Then we can get the pressure by $p = s_{xx} - \sigma$.

$$p^*_L = s^*_{xxL} - \sigma^*_L, \; p^*_R = s^*_{xxR} - \sigma^*_R. \tag{3.41}$$

3.5.3 Case 2: with only the left plastic wave

If $|s_{xxL}| \leq \frac{2}{3}Y_0 \leq |\hat{s}^*_{xxL}|$ and $[(|s_{xxR}| < \frac{2}{3}Y_0$ and $|\hat{s}^*_{xxR}| < \frac{2}{3}Y_0)$ or $(|s_{xxR}| \geq \frac{2}{3}Y_0$ and $|\hat{s}^*_{xxR}| \geq \frac{2}{3}Y_0)]$, there will be only one plastic wave which is in the left. Correspondingly, the Riemann structure of this case is

showed in Fig.2. We need to solve the yielding state of $\widetilde{\boldsymbol{Q}}_L$. The MHLLCEP is given as follows in this case,

$$\boldsymbol{U}_{\text{Case2}}^{\text{MHLLCEP}}(x,t)=\begin{cases}\boldsymbol{U}_L, & \text{if} \quad \dfrac{x}{t}\le \widetilde{s}_L,\\ \widetilde{\boldsymbol{U}}_L, & \text{if} \quad \widetilde{s}_L\le \dfrac{x}{t}\le s_L,\\ \boldsymbol{U}_L^*, & \text{if} \quad s_L\le \dfrac{x}{t}\le s^*,\\ \boldsymbol{U}_R^*, & \text{if} \quad s^*\le \dfrac{x}{t}\le s_R,\\ \boldsymbol{U}_R, & \text{if} \quad \dfrac{x}{t}\ge s_R,\end{cases} \tag{3.42}$$

and the corresonding Eulerian and Lagrangian numerical fluxes are

$$\boldsymbol{F}_{\text{Case2}}^{\text{Euler}}(x,t)=\begin{cases}\boldsymbol{F}_L, & \text{if} \quad \dfrac{x}{t}\le \widetilde{s}_L,\\ \widetilde{\boldsymbol{F}}_L, & \text{if} \quad \widetilde{s}_L\le \dfrac{x}{t}\le s_L,\\ \boldsymbol{F}_L^*, & \text{if} \quad s_L\le \dfrac{x}{t}\le s^*,\\ \boldsymbol{F}_R^*, & \text{if} \quad s^*\le \dfrac{x}{t}\le s_R,\\ \boldsymbol{F}_R, & \text{if} \quad \dfrac{x}{t}\ge s_R,\end{cases} \tag{3.43}$$

$$\boldsymbol{F}_{\text{Case2}}^{\text{Lag}}(x,t)=\begin{cases}\boldsymbol{f}_L^*, & \text{if} \quad s_*\ge \dfrac{x}{t},\\ \boldsymbol{f}_R^*, & \text{if} \quad s^*\le \dfrac{x}{t}.\end{cases} \tag{3.44}$$

According to the Rankine-Hugoniot relation for the left plastic wave, one get

$$\widetilde{\rho}_L(\widetilde{u}_L-\widetilde{s}_L)=\rho_L(u_L-\widetilde{s}_L), \tag{3.45}$$

$$\widetilde{\rho}\widetilde{u}_L(\widetilde{u}_L-\widetilde{s}_L)=\rho_L u_L(u_L-\widetilde{s}_L)+\widetilde{\sigma}_L-\sigma_L, \tag{3.46}$$

$$\widetilde{\rho}\widetilde{E}_L(\widetilde{u}_L-\widetilde{s}_L)=\rho_L E_L(u_L-\widetilde{s}_L)+\widetilde{\sigma}_L\widetilde{u}_L-\sigma_L u_L, \tag{3.47}$$

where $\widetilde{s}_L$ denotes the speed of left plastic wave.

Because the deviatoric stress behind the plastic wave reaches the elastic limit, the deviatoric stress and density are taken as

$$\widetilde{s}_{xxL}=\begin{cases}-\dfrac{2}{3}Y_0, & \text{if} \quad \rho_L^*>\rho_L,\\ \dfrac{2}{3}Y_0, & \text{if} \quad \rho_L^*<\rho_L,\end{cases} \tag{3.48}$$

and

$$\widetilde{\rho}_L=\begin{cases}\rho_L\exp\left(\dfrac{Y_0}{2\mu}+\dfrac{3s_{xxL}}{4\mu}\right) & \text{if} \quad \rho_L^*>\rho_L,\\ \rho_L\exp\left(-\dfrac{Y_0}{2\mu}+\dfrac{3s_{xxL}}{4\mu}\right) & \text{if} \quad \rho_L^*<\rho_L.\end{cases} \tag{3.49}$$

The unknowns are the wave speed $\widetilde{s}_L$, the velocity $\widetilde{u}_L$, the pressure $\widetilde{p}_L$ and the specific internal energy $\widetilde{E}_L$. In the following, we will give the derivations of them.

From Eq.(3.45) we can get the wave speed as

$$\widetilde{s}_L=\frac{\widetilde{\rho}_L\widetilde{u}_L-\rho_L u_L}{\widetilde{\rho}_L-\rho_L}, \tag{3.50}$$

and have the relation of

$$u_L-\widetilde{s}_L=\frac{(u_L-\widetilde{u}_L)\widetilde{\rho}_L}{\widetilde{\rho}_L-\rho_L}. \tag{3.51}$$

Substituting Eq.(3.45) into Eq.(3.46), we have

$$\rho_L(\widetilde{u}_L - u_L)(u_L - \widetilde{s}_L) = \widetilde{\sigma}_L - \sigma_L, \tag{3.52}$$

then substituting Eq.(3.51) into it, we can get the following relation

$$-t(\widetilde{u}_L - u_L)^2 = \widetilde{\sigma}_L - \sigma_L, \tag{3.53}$$

where

$$t = \frac{\rho_L \widetilde{\rho}_L}{\widetilde{\rho}_L - \rho_L}. \tag{3.54}$$

Similar to Eq.(3.52), Eq.(3.46) can be changed into

$$t(u_L - \widetilde{u}_L)(\widetilde{E}_L - E_L) = \widetilde{\sigma}_L \widetilde{u}_L - \sigma_L u_L, \tag{3.55}$$

and we also know that $E = e + \frac{1}{2}u^2$, then we have

$$\widetilde{e}_L - e_L = -\frac{\sigma_L + \widetilde{\sigma}_L}{2t}. \tag{3.56}$$

The EOS (2.4) can be written as

$$e = c_0 p - c_1 f(\rho/\rho_0), \tag{3.57}$$

where $c_0 = \frac{1}{\rho_0 \Gamma_0}$ and $c_1 = \frac{a_0^2}{\Gamma_0}$.

Substituting (3.57) and $\sigma = -p + s_{xx}$ into (3.56), we can get the pressure behind the plastic wave as

$$\widetilde{p}_L = \frac{2t(c_1 f(\widetilde{\rho}_L) + e_L) - (\sigma_L + \widetilde{s}_{xxL})}{2tc_0 - 1}, \tag{3.58}$$

and the Cauchy stress is solved by $\widetilde{\sigma}_L = -\widetilde{p}_L + \widetilde{s}_{xxL}$. Using Eq.(3.53) we can get

$$(\widetilde{u}_L - u_L)^2 = \frac{\sigma_L - \widetilde{\sigma}_L}{t}, \tag{3.59}$$

then the velocity is solved,

$$\widetilde{\boldsymbol{u}}_L = \begin{cases} u_L + \sqrt{\dfrac{\sigma_L - \widetilde{\sigma}_L}{t}} & \text{if } \rho_R^* > \rho_R, \\ u_L - \sqrt{\dfrac{\sigma_L - \widetilde{\sigma}_L}{t}} & \text{if } \rho_R^* < \rho_R. \end{cases} \tag{3.60}$$

After solving the state of $\widetilde{\boldsymbol{Q}}_L$, using the similar process described in Section 3.5.2, the states of $\boldsymbol{Q}_L^*$ and $\boldsymbol{Q}_R^*$ can be worked out as follows.

The contact wave speed is

$$s^* = \frac{\widetilde{\sigma}_L - \sigma_R + \widetilde{\rho}_L \widetilde{u}_L(s_L - \widetilde{u}_L) - \rho_R u_R(s_R - u_R)}{\widetilde{\rho}_L(s_L - \widetilde{u}_L) - \rho_R(s_R - u_R)}, \tag{3.61}$$

The densities are

$$\rho_L^* = \frac{\widetilde{\rho}_L(\widetilde{u}_L - s_L)}{s^* - s_L}, \quad \rho_R^* = \frac{\rho_R(u_R - s_R)}{s^* - s_R}, \tag{3.62}$$

where the left and right elastic wave speeds are evaluted as

$$s_L = \min(\widetilde{u}_L - \widetilde{c}_L, u_R - c_R, 0), \quad s_R = \max(\widetilde{u}_L + \widetilde{c}_L, u_R + c_R, 0). \tag{3.63}$$

The deviatoric stresses are evaluated as

$$\overline{s}_{xxL}^* = \widetilde{s}_{xxL}, \ \ \overline{s}_{xxR}^* = -\frac{4}{3}\mu \ln(\frac{\rho_R^*}{\rho_R}) + s_{xxR}, \tag{3.64}$$

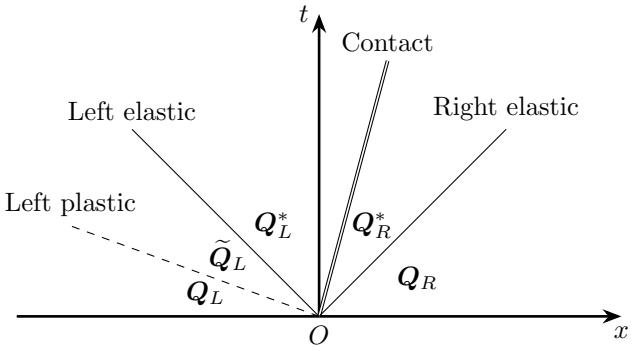

Figure 2: The structures of MHLLCEP method, case 2: with only the left plastic wave.

then using von Mises' yielding condition yields:

$$s_{xxL}^* = \Upsilon(\overline{s}_{xxL}^*), \quad s_{xxR}^* = \Upsilon(\overline{s}_{xxR}^*). \tag{3.65}$$

The Cauchy stresses are given as

$$\sigma_L^* = \sigma_R^* = \widetilde{\sigma}_L - \widetilde{\rho}_L(s_L - \widetilde{u}_L)(s^* - \widetilde{u}_L), \tag{3.66}$$

and the pressures are

$$p_L^* = s_{xxL}^* - \sigma_L^*, \quad p_R^* = s_{xxR}^* - \sigma_R^*. \tag{3.67}$$

3.5.4 Case 3: with only the right plastic wave

If $[(|s_{xxL}| < \frac{2}{3}Y_0$ and $|\hat{s}_{xxL}^*| < \frac{2}{3}Y_0)$ or $(|s_{xxR}| \geq \frac{2}{3}Y_0$ and $|\hat{s}_{xxR}^*| \geq \frac{2}{3}Y_0)]$ and $|s_{xxR}| \leq \frac{2}{3}Y_0 \leq |\hat{s}_{xxR}^*|$, there will be only one plastic wave which is in the right. Correspondingly, the Riemann structure of this case is showed in Fig.3. We need to solve the yielding state of $\widetilde{\boldsymbol{Q}}_R$. The MHLLCEP is given as follows in this case,

$$\boldsymbol{U}_{\text{Case3}}^{\text{MHLLCEP}}(x,t) = \begin{cases} \boldsymbol{U}_L, & \text{if} \quad \dfrac{x}{t} \leq s_L, \\ \boldsymbol{U}_L^*, & \text{if} \quad s_L \leq \dfrac{x}{t} \leq s^*, \\ \boldsymbol{U}_R^*, & \text{if} \quad s^* \leq \dfrac{x}{t} \leq s_R, \\ \widetilde{\boldsymbol{U}}_R, & \text{if} \quad s_R \leq \dfrac{x}{t} \leq \widetilde{s}_R, \\ \boldsymbol{U}_R, & \text{if} \quad \dfrac{x}{t} \geq \widetilde{s}_R, \end{cases} \tag{3.68}$$

and the corresonding Eulerian and Lagrangian numerical flux are

$$\boldsymbol{F}_{\text{Case3}}^{\text{Euler}}(x,t) = \begin{cases} \boldsymbol{F}_L, & \text{if} \quad \dfrac{x}{t} \leq s_L, \\ \boldsymbol{F}_L^*, & \text{if} \quad s_L \leq \dfrac{x}{t} \leq s^*, \\ \boldsymbol{F}_R^*, & \text{if} \quad s^* \leq \dfrac{x}{t} \leq s_R, \\ \widetilde{\boldsymbol{F}}_R, & \text{if} \quad s_R \leq \dfrac{x}{t} \leq \widetilde{s}_R, \\ \boldsymbol{F}_R, & \text{if} \quad \dfrac{x}{t} \geq \widetilde{s}_R, \end{cases} \tag{3.69}$$

$$\boldsymbol{F}_{\text{Case3}}^{\text{Lag}}(x,t) = \begin{cases} \boldsymbol{f}_L^*, & \text{if} \quad s_* \geq \dfrac{x}{t}, \\ \boldsymbol{f}_R^*, & \text{if} \quad s^* \leq \dfrac{x}{t}. \end{cases} \tag{3.70}$$

The deviatoric stress, density and pressure behind the right plastic wave are given as

$$\widetilde{s}_{xxR} = \begin{cases} -\frac{2}{3}Y_0, & \text{if} \quad \rho_R^* > \rho_R, \\ \frac{2}{3}Y_0, & \text{if} \quad \rho_R^* < \rho_R, \end{cases} \quad \widetilde{\rho}_R = \begin{cases} \rho_R \text{exp}\left(\frac{Y_0}{2\mu} + \frac{3s_{xxR}}{4\mu}\right) & \text{if} \quad \rho_R^* > \rho_R, \\ \rho_R \text{exp}\left(-\frac{Y_0}{2\mu} + \frac{3s_{xxR}}{4\mu}\right) & \text{if} \quad \rho_R^* < \rho_R, \end{cases} \tag{3.71}$$

$$\widetilde{p}_R = \frac{2t(c_1 f(\widetilde{\rho}_R) + e_R) - (\sigma_R + \widetilde{s}_{xxR})}{2tc_0 - 1}, \quad t = \frac{\rho_R \widetilde{\rho}_R}{\widetilde{\rho}_R - \rho_R}, \tag{3.72}$$

where $c_0 = \frac{1}{\rho_0 \Gamma_0}$ and $c_1 = \frac{a_0^2}{\Gamma_0}$. The Cauchy stress and velocity are

$$\widetilde{\sigma}_R = -\widetilde{p}_R + \widetilde{s}_{xxR}, \tag{3.73}$$

$$\widetilde{u}_R = \begin{cases} u_R + \sqrt{\frac{\sigma_R - \widetilde{\sigma}_R}{t}} & \text{if} \ \ \rho_R^* > \rho_R, \\ u_R - \sqrt{\frac{\sigma_R - \widetilde{\sigma}_R}{t}} & \text{if} \ \ \rho_R^* < \rho_R. \end{cases} \tag{3.74}$$

After obtaining the state of $\widetilde{\boldsymbol{Q}}_R$, we can solve the states of $\boldsymbol{Q}_L^*$ and $\boldsymbol{Q}_R^*$.
The contact wave speed is

$$s^* = \frac{\sigma_L - \widetilde{\sigma}_R + \rho_L u_L(s_L - u_L) - \widetilde{\rho}_R \widetilde{u}_R(s_R - \widetilde{u}_R)}{\rho_L(s_L - u_L) - \widetilde{\rho}_R(s_R - \widetilde{u}_R)}. \tag{3.75}$$

The densities are

$$\rho_L^* = \frac{\rho_L(u_L - s_L)}{s^* - s_L}, \quad \rho_R^* = \frac{\widetilde{\rho}_R(\widetilde{u}_R - s_R)}{s^* - s_R}, \tag{3.76}$$

where the left and right elastic wave speeds are

$$s_L = \min(u_L - c_L, \widetilde{u}_R - \widetilde{c}_R, 0), \quad s_R = \max(u_L + c_L, \widetilde{u}_R + \widetilde{c}_R, 0). \tag{3.77}$$

The deviatoric stresses are

$$\overline{s}_{xxL}^* = -\frac{4}{3}\mu \ln(\frac{\rho_L^*}{\rho_L}) + s_{xxL}, \ \ \overline{s}_{xxR}^* = \widetilde{s}_{xxR}, \tag{3.78}$$

$$s_{xxL}^* = \Upsilon(\overline{s}_{xxL}^*), \quad s_{xxR}^* = \Upsilon(\overline{s}_{xxR}^*). \tag{3.79}$$

The Cauchy stresses are

$$\sigma_L^* = \sigma_R^* = \sigma_L - \rho_L(s_L - u_L)(s^* - u_L), \tag{3.80}$$

and the pressures are

$$p_L^* = s_{xxL}^* - \sigma_L^*, \quad p_R^* = s_{xxR}^* - \sigma_R^*. \tag{3.81}$$

3.5.5 Case 4: with both the left and right plastic waves

If $|s_{xxL}| \leq \frac{2}{3}Y_0 \leq |\hat{s}_{xxL}^*|$ and $|s_{xxR}| \leq \frac{2}{3}Y_0 \leq |\hat{s}_{xxR}^*|$. There are two plastic waves showed in Fig.4. For this case, the MHLLCEP Riemann solver is given as

$$\boldsymbol{U}_{\text{Case4}}^{\text{MHLLCEP}}(x,t) = \begin{cases} \boldsymbol{U}_L, & \text{if} \quad \frac{x}{t} \leq s_L, \\ \boldsymbol{U}_L^*, & \text{if} \quad s_L \leq \frac{x}{t} \leq \widetilde{s}_L, \\ \widetilde{\boldsymbol{U}}_L, & \text{if} \quad \widetilde{s}_L \leq \frac{x}{t} \leq s^*, \\ \widetilde{\boldsymbol{U}}_R, & \text{if} \quad s^* \leq \frac{x}{t} \leq \widetilde{s}_R, \\ \boldsymbol{U}_R^*, & \text{if} \quad \widetilde{s}_R \leq \frac{x}{t} \leq s_R, \\ \boldsymbol{U}_R, & \text{if} \quad \frac{x}{t} \geq s_R, \end{cases} \tag{3.82}$$

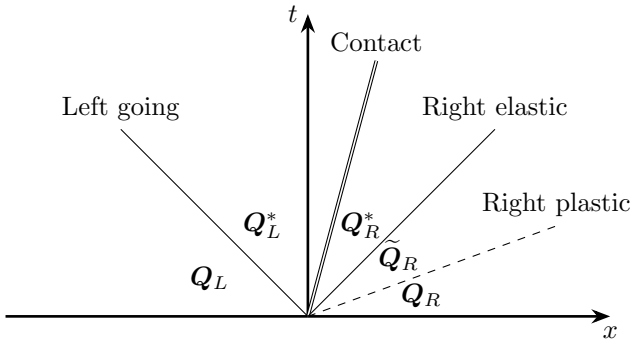

Figure 3: The structures of HLLCEP method, case 3: with only the right plastic wave.

and the corresonding Eulerian and Lagrangian numerical flux are

$$\boldsymbol{F}^{\text{Euler}}_{\text{Case4}}(x,t) = \begin{cases} \boldsymbol{F}_L, & \text{if} \quad \dfrac{x}{t} \le s_L, \\ \boldsymbol{F}_L^*, & \text{if} \quad \widetilde{s}_L \le \dfrac{x}{t} \le s_L, \\ \widetilde{\boldsymbol{F}}_L, & \text{if} \quad s_L \le \dfrac{x}{t} \le s^*, \\ \widetilde{\boldsymbol{F}}_R, & \text{if} \quad s^* \le \dfrac{x}{t} \le s_R, \\ \boldsymbol{F}_R^*, & \text{if} \quad s_R \le \dfrac{x}{t} \le \widetilde{s}_R, \\ \boldsymbol{F}_R, & \text{if} \quad \dfrac{x}{t} \ge s_R, \end{cases} \tag{3.83}$$

$$\boldsymbol{F}^{\text{Lag}}_{\text{Case4}}(x,t) = \begin{cases} \widetilde{\boldsymbol{f}}_L, & \text{if} \quad s_* \ge \dfrac{x}{t}, \\ \widetilde{\boldsymbol{f}}_R, & \text{if} \quad s^* \le \dfrac{x}{t}. \end{cases} \tag{3.84}$$

The states of $\widetilde{\boldsymbol{Q}}_L$ and $\widetilde{\boldsymbol{Q}}_R$ can be solved in the same way with Section 3.5.3 and Section 3.5.4. Then the states of $\boldsymbol{Q}_L^*$ and $\boldsymbol{Q}_R^*$ are given as following.

The speed of waves are evaluted as

$$s_L = \min(\widetilde{u}_L - \widetilde{c}_L, \widetilde{u}_R - \widetilde{c}_R, 0), \quad s_R = \max(\widetilde{u}_L + \widetilde{c}_L, \widetilde{u}_R + \widetilde{c}_R, 0), \tag{3.85}$$

$$s^* = \frac{\widetilde{\sigma}_L - \widetilde{\sigma}_R + \widetilde{\rho}_L\widetilde{u}_L(s_L - \widetilde{u}_L) - \widetilde{\rho}_R\widetilde{u}_R(s_R - \widetilde{u}_R)}{\widetilde{\rho}_L(s_L - \widetilde{u}_L) - \widetilde{\rho}_R(s_R - \widetilde{u}_R)}. \tag{3.86}$$

Thanks to Eq.(3.76), the densities behind the left and right plastic waves are given as ,

$$\rho_L^* = \frac{\widetilde{\rho}_L(\widetilde{u}_L - s_L)}{s^* - s_L}, \quad \rho_R^* = \frac{\widetilde{\rho}_R(\widetilde{u}_R - s_R)}{s^* - s_R}, \tag{3.87}$$

and the deviatoric stresses are given as

$$\overline{s}^*_{xxL} = \widetilde{s}_{xxL}, \tag{3.88}$$
$$\overline{s}^*_{xxR} = \widetilde{s}_{xxR}, \tag{3.89}$$
$$\tag{3.90}$$

then using the von Mises' yielding condition yields

$$s^*_{xxL} = \Upsilon(\overline{s}^*_{xxL}), \quad s^*_{xxR} = \Upsilon(\overline{s}^*_{xxR}). \tag{3.91}$$

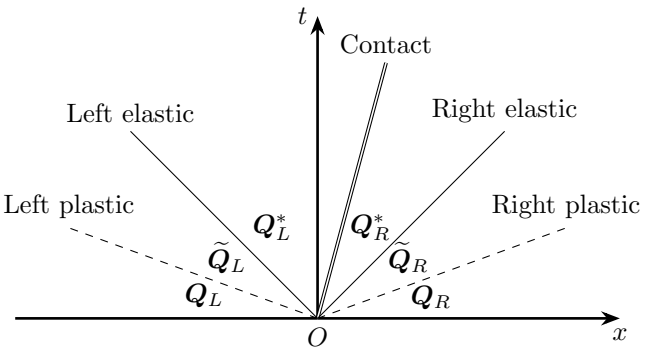

Figure 4: The structures of MHLLCEP method, case 4: with both left and right plastic waves.

The Cauchy stresses are solved as

$$\sigma_L^* = \sigma_R^* = \widetilde{\sigma}_L - \widetilde{\rho_L}(s_L - \widetilde{u}_L)(s^* - \widetilde{u}_L). \tag{3.92}$$

So we can get the pressure by $p = s_{xx} - \sigma$,

$$p_L^* = s_{xxL}^* - \sigma_L^*, \quad p_R^* = s_{xxR}^* - \sigma_R^*. \tag{3.93}$$

3.6 Summary of MHLLCEP

Here, we present all the procedures of MHLLCEP in a more simple way.

1. Assume there is no plastic wave in the Riemann solvers. Based on this assumption, we perform the following evaluations:

   (a) evaluate $\hat{s}^*$

   $$\hat{s}^* = \frac{\sigma_L - \sigma_R + \rho_L u_L(s_L - u_L) - \rho_R u_R(s_R - u_R)}{\rho_L(s_L - u_L) - \rho_R(s_R - u_R)}.$$

   (b) Evaluate $\hat{\rho}_L^*$ and $\hat{\rho}_R^*$

   $$\hat{\rho}_L^* = \frac{\rho_L(u_L - s_L)}{s^* - s_L}, \quad \hat{\rho}_R^* = \frac{\rho_R(u_R - s_R)}{s^* - s_R}.$$

   (c) Evaluate the deviatoric stress

   $$\hat{s}_{xxL}^* = -\frac{4}{3}\mu \ln(\frac{\hat{\rho}_L^*}{\rho_L}) + s_{xxL}, \;\; \hat{s}_{xxR}^* = -\frac{4}{3}\mu \ln(\frac{\hat{\rho}_R^*}{\rho_R}) + s_{xxR}.$$

   (d) Evaluate the pressure

2. Decide whether the state reached the elastic limit or not

   (a) If $|s_{xxL}| < \frac{2}{3}Y_0 \le |\hat{s}_{xxL}^*|$, the left plastic wave exists, we need to evaluate the left yielding state. The deviatoric stress, density and pressure behind the left plastic wave are given as

   $$\widetilde{s}_{xxL} = \begin{cases} -\dfrac{2}{3}Y_0, & \text{if} \quad \rho_L^* > \rho_L, \\ \dfrac{2}{3}Y_0, & \text{if} \quad \rho_L^* < \rho_L, \end{cases} \quad \widetilde{\rho}_L = \begin{cases} \rho_L \exp\left(\dfrac{Y_0}{2\mu} + \dfrac{3s_{xxL}}{4\mu}\right) & \text{if} \quad \rho_L^* > \rho_L, \\ \rho_L \exp\left(-\dfrac{Y_0}{2\mu} + \dfrac{3s_{xxL}}{4\mu}\right) & \text{if} \quad \rho_L^* < \rho_L, \end{cases}$$

   $$\widetilde{p}_L = \frac{2t(c_1 f(\widetilde{\rho}_L) + e_L) - (\sigma_L + \widetilde{s}_{xxL})}{2tc_0 - 1}, \quad t = \frac{\rho_L \widetilde{\rho}_L}{\widetilde{\rho}_L - \rho_L},$$

and the Cauchy stress and velocity are

$$\widetilde{\sigma}_L = -\widetilde{p}_L + \widetilde{s}_{xxL},$$

$$\widetilde{u}_L = \begin{cases} u_L - \sqrt{\dfrac{\sigma_L - \widetilde{\sigma}_L}{t}} & \text{if } \rho_L^* > \rho_L, \\ u_L + \sqrt{\dfrac{\sigma_L - \widetilde{\sigma}_L}{t}} & \text{if } \rho_L^* < \rho_L. \end{cases}$$

If the left plastic wave does not exist,

$$\widetilde{\boldsymbol{Q}}_L = \boldsymbol{Q}_L.$$

(b) If $|s_{xxR}| < \frac{2}{3}Y_0 \leq |\hat{s}^*_{xxR}|$, right plastic wave exists, we need to evaluate the right yielding state. The deviatoric stress, density and pressure behind the right plastic wave are given as

$$\widetilde{s}_{xxR} = \begin{cases} -\dfrac{2}{3}Y_0, & \text{if } \rho_R^* > \rho_R, \\ \dfrac{2}{3}Y_0, & \text{if } \rho_R^* < \rho_R, \end{cases} \quad \widetilde{\rho}_R = \begin{cases} \rho_R \exp\left(\dfrac{Y_0}{2\mu} + \dfrac{3s_{xxR}}{4\mu}\right) & \text{if } \rho_R^* > \rho_R, \\ \rho_R \exp\left(-\dfrac{Y_0}{2\mu} + \dfrac{3s_{xxR}}{4\mu}\right) & \text{if } \rho_R^* < \rho_R, \end{cases}$$

$$\widetilde{p}_R = \frac{2t(c_1 f(\widetilde{\rho}_R) + e_R) - (\sigma_R + \widetilde{s}_{xxR})}{2tc_0 - 1}, \quad t = \frac{\rho_R \widetilde{\rho}_R}{\widetilde{\rho}_R - \rho_R},$$

and the Cauchy stress and velocity are

$$\widetilde{\sigma}_R = -\widetilde{p}_R + \widetilde{s}_{xxR},$$

$$\widetilde{u}_R = \begin{cases} u_R + \sqrt{\dfrac{\sigma_R - \widetilde{\sigma}_R}{t}} & \text{if } \rho_R^* > \rho_R, \\ u_R - \sqrt{\dfrac{\sigma_R - \widetilde{\sigma}_R}{t}} & \text{if } \rho_R^* < \rho_R. \end{cases}$$

If right plactic wave does not exist,

$$\widetilde{\boldsymbol{Q}}_R = \boldsymbol{Q}_R.$$

3. re-evaluate the states in the star regions

(a) Solve the wave speeds,

$$s_L = \min(\widetilde{u}_L - \widetilde{c}_L, \widetilde{u}_R - \widetilde{c}_R, 0), \quad s_R = \max(\widetilde{u}_L + \widetilde{c}_L, \widetilde{u}_R + \widetilde{c}_R, 0),$$

$$s^* = \frac{\widetilde{\sigma}_L - \widetilde{\sigma}_R + \widetilde{\rho}_L \widetilde{u}_L (s_L - \widetilde{u}_L) - \widetilde{\rho}_R \widetilde{u}_R (s_R - \widetilde{u}_R)}{\widetilde{\rho}_L (s_L - \widetilde{u}_L) - \widetilde{\rho}_R (s_R - \widetilde{u}_R)}.$$

(b) Solve the densities,

$$\rho_L^* = \frac{\widetilde{\rho}_L (\widetilde{u}_L - s_L)}{s^* - s_L}, \quad \rho_R^* = \frac{\widetilde{\rho}_R (\widetilde{u}_R - s_R)}{s^* - s_R},$$

(c) Solve the deviatoric stresses,

$$\widetilde{s}^*_{xxL} = \begin{cases} \widetilde{s}_{xxL} & if\ |\hat{s}^*_{xxL}| \geq \frac{2}{3}Y_0 \\ -\frac{4}{3}\mu \ln\left(\frac{\rho_L^*}{\widetilde{\rho}_L}\right) + \widetilde{s}_{xxL} & otherwise \end{cases},$$

$$\widetilde{s}^*_{xxR} = \begin{cases} \widetilde{s}_{xxR} & if\ |\hat{s}^*_{xxR}| \geq \frac{2}{3}Y_0 \\ -\frac{4}{3}\mu \ln\left(\frac{\rho_R^*}{\widetilde{\rho}_R}\right) + \widetilde{s}_{xxR} & otherwise \end{cases},$$

then using the von Mises' yielding condition yields

$$s^*_{xxL} = \Upsilon(\widetilde{s}^*_{xxL}), \quad s^*_{xxR} = \Upsilon(\widetilde{s}^*_{xxR}).$$

(d) Solving the Cauchy stresses:

$$\sigma_L^* = \sigma_R^* = \widetilde{\sigma}_L - \widetilde{\rho_L}(s_L - \widetilde{u}_L)(s^* - \widetilde{u}_L).$$

(e) The pressure is given by $p = s_{xx} - \sigma$.

4 A High-order cell-centered Lagrangian scheme for 1D conservative hydrodynamic equations with Wilkins' model

Here, we consider the following governing equations with Wilkins' model and von Mises' yielding condition

$$\begin{cases} \partial_t \rho + \partial_x(\rho u) = 0, \\ \partial_t(\rho u) + \partial_x(\rho u^2 + p - s_{xx}) = 0, \\ \partial_t(\rho E) + \partial_x([\rho E + p - s_{xx}]u) = 0, \\ \partial_t s_{xx} + u\partial_x s_{xx} - \dfrac{4}{3}\partial_x u = 0, \\ |s_{xx}| \le \dfrac{2}{3}Y_0, \end{cases} \tag{4.1}$$

where $Q = (\rho, \rho u, \rho E, s_{xx})^T$. For a Lagrangian scheme, the governing equations also include the equation for moving the coordinates at the vertex of the mesh,

$$\frac{dx(t)}{dt} = u(x,t). \tag{4.2}$$

The spatial domain is discretized into N cells $I_i = [x_{i-1/2}, x_{i+1/2}]$ of space sizes $\Delta x_i = x_{i+1/2} - x_{i-1/2}$ for $i = 1, 2, \cdots, N$. For a given cell I_i, the cell center is denoted by x_i. The velocity $u_{i+1/2}$ is defined at the vertex of the mesh. The value of the cell average for the cell I_i is defined by

$$\overline{\boldsymbol{Q}}_i = \frac{1}{\Delta x_i}\int_{I_i} \boldsymbol{Q} dx. \tag{4.3}$$

4.1 Spatial discretization

The semi-discrete finite volume scheme of the conservative equations (4.1) in the cell I_i is written as

$$\frac{d(\overline{\boldsymbol{U}}_i \Delta x_i)}{dt} = -(\boldsymbol{F}_{i+\frac{1}{2}} - \boldsymbol{F}_{i-\frac{1}{2}}), \tag{4.4}$$

where

$$\boldsymbol{F}_{i+\frac{1}{2}} = \boldsymbol{\Phi}(\boldsymbol{Q}_{L,i+\frac{1}{2}}, \boldsymbol{Q}_{R,i+\frac{1}{2}}) = \begin{bmatrix} 0 \\ p_{i+\frac{1}{2}} - (s_{xx})_{i+\frac{1}{2}} \\ (p_{i+\frac{1}{2}} - (s_{xx})_{i+\frac{1}{2}})u_{i+\frac{1}{2}} \end{bmatrix}, \tag{4.5}$$

$\boldsymbol{Q}_{L,i+\frac{1}{2}}$ and $\boldsymbol{Q}_{R,i+\frac{1}{2}}$ represent the left and right values of $\boldsymbol{Q}$ at the cell's boundary $x_{i+\frac{1}{2}}$, and $p_{i+\frac{1}{2}}$, $(s_{xx})_{i+\frac{1}{2}}$ and $u_{i+\frac{1}{2}}$ denote the Godunov values at $x_{i+\frac{1}{2}}$, respectively.

The Godunov values $\boldsymbol{Q}_{i+\frac{1}{2}}$ can be solved by the Riemiann problem (3.1) at $x_{i+\frac{1}{2}}$,

$$\boldsymbol{Q}_{i+\frac{1}{2}} = \begin{cases} \boldsymbol{Q}_L^*, & \text{if } \dfrac{dx}{dt} \le s^*, \\ \boldsymbol{Q}_R^*, & \text{if } \dfrac{dx}{dt} > s^*, \end{cases} \tag{4.6}$$

where $\boldsymbol{Q}_L^*$, $\boldsymbol{Q}_R^*$ and s^* are evaluated by the MHLLCEP in Section 3.

Before this, we must give the left and right initial values ($\boldsymbol{Q}_{L,i+\frac{1}{2}}$ and $\boldsymbol{Q}_{R,i+\frac{1}{2}}$) by the cell average value $\overline{\boldsymbol{Q}}$ ($i = 1, 2, \cdots, N$). This process is done by the spatial reconstruction.

4.1.1 High-order reconstruction

The construction is carried out in the characteristic variables space in this paper, which is more stable and accurate than reconstructing in the primitive variables space or the conservative variables space.

First, we transform the conservative variables to local characteristic variables,

$$\boldsymbol{W} = \boldsymbol{L} \cdot \overline{\boldsymbol{Q}}, \tag{4.7}$$

where $\boldsymbol{L}$ is the left eigenvector of $\boldsymbol{J}$, and $\boldsymbol{J}_i$ is the Jacobian matrix (3.3) in I_i.

Here, based on the cell average of $\mathbf{W}$, we first use the third-order modified WENO scheme constructed in Ref.([13]) to reconstruct the characteristic variables at the left and right interfaces ($\boldsymbol{W}_L$ and $\boldsymbol{W}_R$) of every cell and then project the reconstructed values of $\mathbf{W}$ back to the conservative variables space,

$$\boldsymbol{Q}_L = \boldsymbol{R} \cdot \boldsymbol{W}_L, \quad \boldsymbol{Q}_R = \boldsymbol{R} \cdot \boldsymbol{W}_R, \tag{4.8}$$

where $\boldsymbol{R}$ is the right eigenvector of $\boldsymbol{J}$.

4.1.2 Spatial discretization of the constitutive equation

In the Lagrangian frame, the equation of the constitute model (2.8) can be written as

$$\frac{ds_{xx}}{dt} = \frac{4\mu}{3}\frac{\partial u}{\partial x}, \tag{4.9}$$

In order to satisfy the geometrical conservation law, the volume of the cell I_i is evaluated by

$$V_i(t) = x_{i+\frac{1}{2}}(t) - x_{i-\frac{1}{2}}(t). \tag{4.10}$$

Taking the material derivative at both sides, we can get

$$\dot{V}_i(t) = \dot{x}_{i+\frac{1}{2}}(t) - \dot{x}_{i-\frac{1}{2}}(t), \tag{4.11}$$

as a result of (4.2), it becomes

$$\dot{V}_i(t) = u_{i+\frac{1}{2}}(t) - u_{i-\frac{1}{2}}(t), \tag{4.12}$$

combining (4.10), it becomes

$$\frac{\dot{V}_i(t)}{V_i} = \frac{u_{i+\frac{1}{2}}(t) - u_{i-\frac{1}{2}}(t)}{x_{i+\frac{1}{2}}(t) - x_{i-\frac{1}{2}}(t)}, \tag{4.13}$$

By using Eq.(2.7), we can get

$$\frac{\partial u}{\partial x} = \frac{u_{i+\frac{1}{2}}(t) - u_{i-\frac{1}{2}}(t)}{x_{i+\frac{1}{2}}(t) - x_{i-\frac{1}{2}}(t)}. \tag{4.14}$$

Then the discretization of the constitutive equation is given as

$$\frac{ds_{xx}}{dt} = \frac{4\mu}{3}\frac{u_{i+\frac{1}{2}}(t) - u_{i-\frac{1}{2}}(t)}{x_{i+\frac{1}{2}}(t) - x_{i-\frac{1}{2}}(t)}. \tag{4.15}$$

4.1.3 Reconstruction near the Multi-material interface

Using a high-order spatial scheme such as the third-order WENO scheme, reconstructing cross the interface may cause oscillations. So we need to do some special treatment near the interface. First, we track the interface by adding a marker function Mrk_i to mark the material in every cell. For two materials problem, we can initial Mrk as

$$\begin{cases} \mathrm{Mrk}(i) = 0, & \text{if cell } i \text{ is material A}, \\ \mathrm{Mrk}(i) = 1, & \text{if cell } i \text{ is material B}, \end{cases} \tag{4.16}$$

and we can get the interface is between cell ii and $ii+1$, if $\mathrm{Mrk}_{ii} = 0$ and $\mathrm{Mrk}_{ii+1} = 1$.

Using the reconstruction in the left side of the interface as an example. Constructing $\boldsymbol{W}_R(ii - \frac{1}{2})$ and $\boldsymbol{W}_L(ii + \frac{1}{2})$ are both with the stencil of $S^3 = (I_{ii-1}, I_{ii}, I_{ii+1})$, where cell I_{ii+1} is on the other side of the interface with a different EOS. Showed in Fig.5, we treat the interface as a special boundary and a ghost cell I'_{ii+1} is added on the right side to replace the use of I_{ii+1}.

The cell average values of the ghost cell I'_{ii+1} is given as follows, the Cauchy stress and the velocity are continuous across the interface according to the relations in Eq.(3.18), so we use the real values on cell I_{ii+1}

$$\overline{\sigma}'_{ii+1} = \overline{\sigma}_{ii+1}, \quad \overline{u}'_{ii+1} = \overline{u}_{ii+1}. \tag{4.17}$$

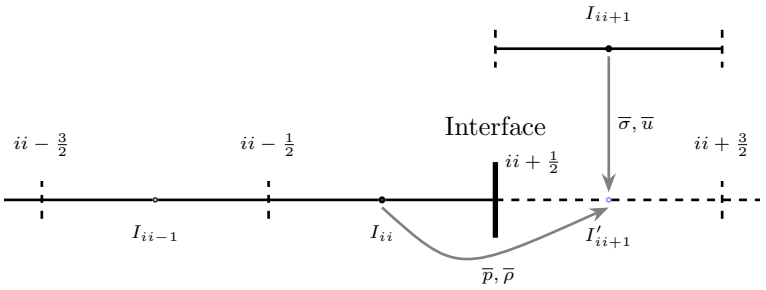

Figure 5: Ghost cell near the interface.

However, the values of pressure and density are not continuous, so we use a reflected condition on the interface as

$$\overline{p}'_{ii+1} = \overline{p}_{ii}, \quad \overline{\rho}'_{ii+1} = \overline{\rho}_{ii}. \tag{4.18}$$

After we get all the primitive variables on the ghost cell I'_{ii+1}, using the EOS of material A on the left, we can get all the conservative variables $\boldsymbol{Q}'_{ii+1}$ and the characteristic variables $\boldsymbol{W}'_{ii+1}$ with the same process in Eq.(4.7). With the variables of $\boldsymbol{W}_{ii-1}$, $\boldsymbol{W}_{ii}$ and $\boldsymbol{W}'_{ii+1}$, we can reconstruct $\boldsymbol{W}_R(ii-\frac{1}{2})$ and $\boldsymbol{W}_L(ii+\frac{1}{2})$, respectively.

On the right side with the EOS of material B, setting a ghost cell of I'_{ii} in the stencil $S^3 = (I'_{ii}, I_{ii+1}, I_{ii+2})$ and using a similar process, we can get new reconstructions of $\boldsymbol{W}_R(ii+\frac{1}{2})$ and $\boldsymbol{W}_L(ii+\frac{3}{2})$, respectively.

4.2 Time discretization

We use the third-order TVD-Runge-Kutta method as the time marching method, the TVD-Runge-Kutta method used in the Lagrangian schemes with von Mises' yielding condition is given in Ref.([12]) as follows.

Step 1,

$$\begin{aligned}
&x^{(1)}_{i+\frac{1}{2}} = x^{(0)}_{i+\frac{1}{2}} + \Delta t^n u^{(0)}_{i+\frac{1}{2}},\\
&\Delta x^{(1)}_i = x^{(1)}_{i+\frac{1}{2}} - x^{(1)}_{i-\frac{1}{2}},\\
&\Delta x^{(1)}_i \overline{\boldsymbol{U}}^{(1)}_i = \Delta x^{(0)}_i \overline{\boldsymbol{U}}^{(0)}_i + \Delta t^n \boldsymbol{L}(\overline{U}^{(0)}_i, (\overline{s_{xx}})^{(0)}_i, x^{(0)}_{i+\frac{1}{2}}),\\
&(\overline{\hat{s}_{xx}})^{(1)}_i = (\overline{s_{xx}})^{(0)}_i + \Delta t^n \Theta(u^{(0)}_{i+\frac{1}{2}}, x^{(0)}_{i+\frac{1}{2}}),\\
&(\overline{s_{xx}})^{(1)}_i = \Upsilon((\overline{\hat{s}_{xx}})^{(1)}_i).
\end{aligned} \tag{4.19}$$

Step 2,

$$\begin{aligned}
&x^{(2)}_{i+\frac{1}{2}} = \frac{3}{4} x^{(0)}_{i+\frac{1}{2}} + \frac{1}{4}\left(x^{(1)}_{i+\frac{1}{2}} + \Delta t^n u^{(1)}_{i+\frac{1}{2}}\right),\\
&\Delta x^{(2)}_i = x^{(2)}_{i+\frac{1}{2}} - x^{(2)}_{i-\frac{1}{2}},\\
&\Delta x^{(2)}_i \overline{\boldsymbol{U}}^{(2)}_i = \frac{3}{4}\Delta x^{(0)}_i \overline{\boldsymbol{U}}^{(0)}_i + \frac{1}{4}\left(\Delta x^{(1)}_i \overline{\boldsymbol{U}}^{(1)}_i + \Delta t^n \boldsymbol{L}(\overline{U}^{(1)}_i, (\overline{s_{xx}})^{(1)}_i, x^{(1)}_{i+\frac{1}{2}}\right),\\
&(\overline{\hat{s}_{xx}})^{(2)}_i = \frac{3}{4}(\overline{s_{xx}})^{(0)}_i + \frac{1}{4}\left((\overline{s_{xx}})^{(1)}_i + \Delta t^n \Theta(u^{(1)}_{i+\frac{1}{2}}, x^{(1)}_{i+\frac{1}{2}})\right),\\
&(\overline{s_{xx}})^{(2)}_i = \Upsilon((\overline{\hat{s}_{xx}})^{(2)}_i).
\end{aligned} \tag{4.20}$$

Step 3,

$$
\begin{aligned}
&x_{i+\frac{1}{2}}^{(3)} = \frac{1}{3}x_{i+\frac{1}{2}}^{(0)} + \frac{2}{3}\left(x_{i+\frac{1}{2}}^{(2)} + \Delta t^n u_{i+\frac{1}{2}}^{(2)}\right),\\
&\Delta x_i^{(3)} = x_{i+\frac{1}{3}}^{(2)} - x_{i-\frac{1}{2}}^{(3)},\\
&\Delta x_i^{(3)}\overline{\boldsymbol{U}}_i^{(2)} = \frac{1}{3}\Delta x_i^{(0)}\overline{\boldsymbol{U}}_i^{(0)} + \frac{2}{3}\left(\Delta x_i^{(1)}\overline{\boldsymbol{U}}_i^{(2)} + \Delta t^n \boldsymbol{L}(\overline{U}_i^{(2)}, (\overline{s_{xx}})_i^{(2)}, x_{i+\frac{1}{2}}^{(2)}\right),\\
&(\overline{\hat{s}_{xx}})_i^{(3)} = \frac{1}{3}(\overline{s_{xx}})_i^{(0)} + \frac{2}{3}\left((\overline{s_{xx}})_i^{(2)} + \Delta t^n \Theta(u_{i+\frac{1}{2}}^{(2)}, x_{i+\frac{1}{2}}^{(2)})\right),\\
&(\overline{s_{xx}})_i^{(3)} = \Upsilon((\overline{\hat{s}_{xx}})_i^{(3)}).
\end{aligned}
\tag{4.21}
$$

Where $\boldsymbol{L}$ and Θ are the numerical spatial operators representing the right hands of Eq.(4.4) and Eq.(4.15), respectively, and the variables with the superscripts n and $n+1$ denote the values of the corresponding variables at the n-th and $(n+1)$-th time steps, respectively.

5 Numerical tests

In this section, our MHLLCEP Riemann solver is tested in different problems to see the capability of capturing elastic and plastic waves, especially in the problems with different materials interface.

5.1 Accuracy test

In the first test, a smooth solution is used to test the accuracy of the scheme. The computational domian is $[0, 1]$, and a periodic boundary condition is used. The EOS is given by the Mie-Grüneisen model with the parameters $\rho_0 = 8930\text{kg/m}^3$, $a_0 = 3940\text{m/s}$, $\Gamma_0 = 2$, and $s = 1.49$. The constitutive model has the following parameters, $\mu = 4.5 \times 10^{10}\text{Pa}$ and $Y^0 = 9 \times 10^{10}\text{Pa}$. The initial condition is given as

$$
\rho = \rho_0(1 - b\sin(2\pi x)), \quad u = a, \quad p = 1.1\rho u^2, \quad s_{xx} = s_0\sin(2\pi x), \tag{5.1}
$$

where $a = 10,000\text{m/s}$, $b = 0.1$ and $s_0 = 6 \times 10^5\text{Pa}$.

The final results are given at time $t = 1 \times 10^{-4}$. The reference result is computed with a refined mesh of $N = 2000$, the L_1- and L_∞-norm errors are showed in Table 5.1. We can see that, with a modified third-order WENO scheme, the high-order cell-centered Lagrangian scheme can achieve the designed accuracy.

Table 5.1: The accuracy with smooth solution.

	N	L_1 error	L_1 order	L_∞ error	L_∞ order
ρ	50	7.74×10^{-5}	—	3.34×10^{-4}	—
	100	9.84×10^{-6}	2.97	3.47×10^{-5}	3.27
	200	1.40×10^{-6}	2.81	6.85×10^{-6}	2.34
	400	2.25×10^{-7}	2.63	1.33×10^{-6}	2.36
s_{xx}	50	8.21×10^{-4}	—	3.55×10^{-3}	—
	100	1.04×10^{-4}	2.98	3.68×10^{-4}	3.27
	200	1.48×10^{-5}	2.81	7.27×10^{-5}	2.33
	400	2.39×10^{-6}	2.63	1.42×10^{-5}	2.36

5.2 Piston problem

In the second test, we consider the piston problem [14] with a piece of copper with the initial condition of

$$
\rho = 8930\text{kg/m}^3, \quad p = 10^5\text{Pa}, \quad u = 0\text{m/s}, \quad s_{xx} = 0\text{Pa}. \tag{5.2}
$$

The EOS for copper is given by the Mie-Grüneisen model with the parameters

$$
\rho_0 = 8930\text{kg/m}^3, \quad a_0 = 3940\text{m/s}, \quad ,\Gamma_0 = 2, \quad s = 1.49. \tag{5.3}
$$

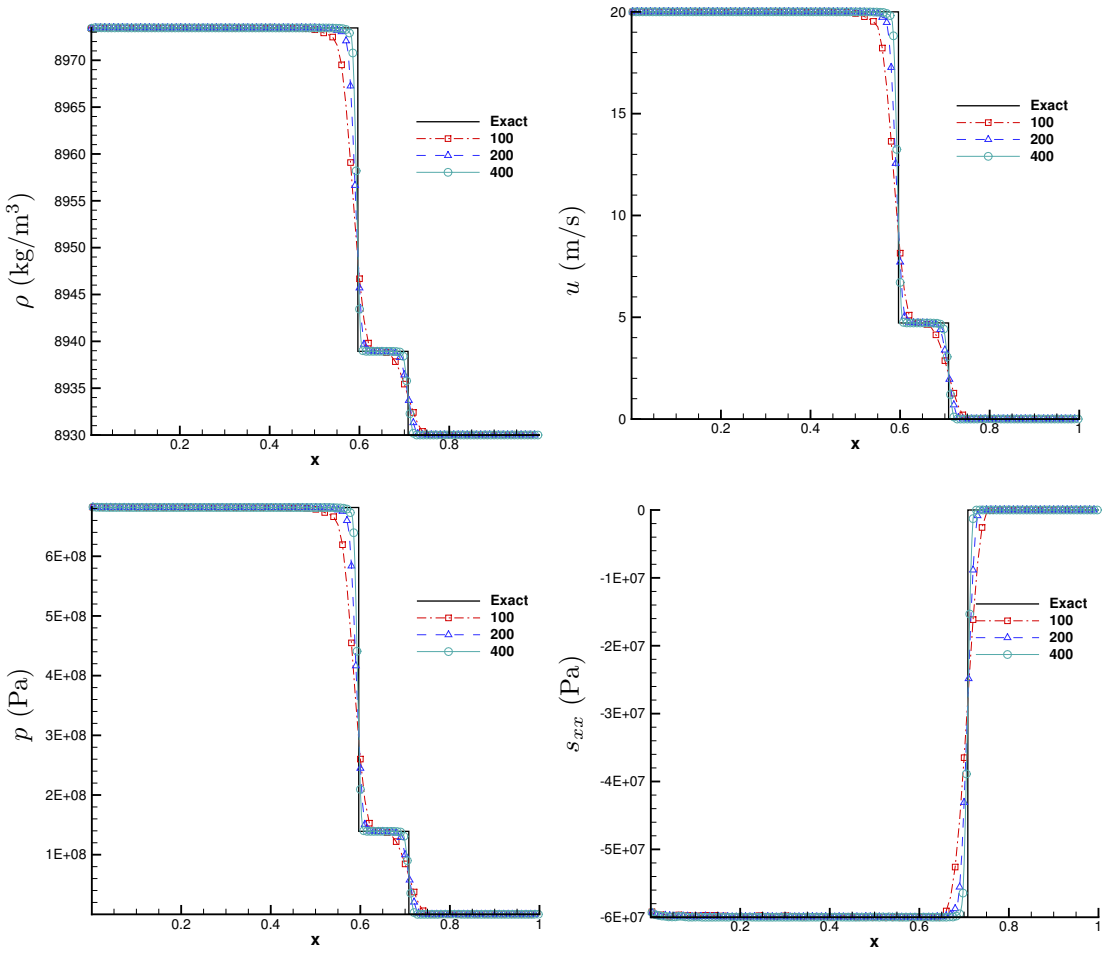

Figure 6: The result of Piston problem

The constitutive model is characterized by the following parameters,

$$\mu = 4.5 \times 10^{10}\text{Pa}, \quad Y_0 = 9 \times 10^{7}\text{Pa}. \tag{5.4}$$

We use the velocity boundary condition with $u_{\text{piston}} = 20\text{m/s}$ on the left boundary and a wall boundary condition on the right boundary.

In Fig.6, we test the convergence of the scheme with different meshes of 100, 200 and 400 cells. The final time is $t = 150\mu s$. We can see that the current scheme can capture the leading elastic shock wave and the followed plastic wave well without numerical oscillation.

5.3 Wilkins' problem

This problem, first introduced by Wilkins, is used to test the ability of capturing rarefaction waves of a scheme. In this problem, a moving aluminium plate striking on another aluminium plate. The EOS for aluminium is given by the Mie-Grüneisen model with the parameters $\rho_0 = 2785\text{kg/m}^3$, $a_0 = 5328\text{m/s}$, $\Gamma_0 = 2$ and $s = 1.338$. The constitutive model is characterized by the parameters $\mu = 2.76 \times 10^{10}\text{Pa}$ and $Y_0 = 3 \times 10^{8}\text{Pa}$. The initial conditions are given as

$$\begin{cases} \rho = 2785\text{kg/m}^3, \quad u = 800\text{m/s}, \quad p = 10^{-6}\text{Pa}, \quad \text{if} \quad 0\text{m} \le x \le 5 \times 10^{-3}\text{m}, \\ \rho = 2785\text{kg/m}^3, \quad u = 0\text{m/s}, \quad p = 10^{-6}\text{Pa}, \quad \text{if} \quad 5 \times 10^{-3}\text{m} \le x \le 50 \times 10^{-3}\text{m}. \end{cases} \tag{5.5}$$

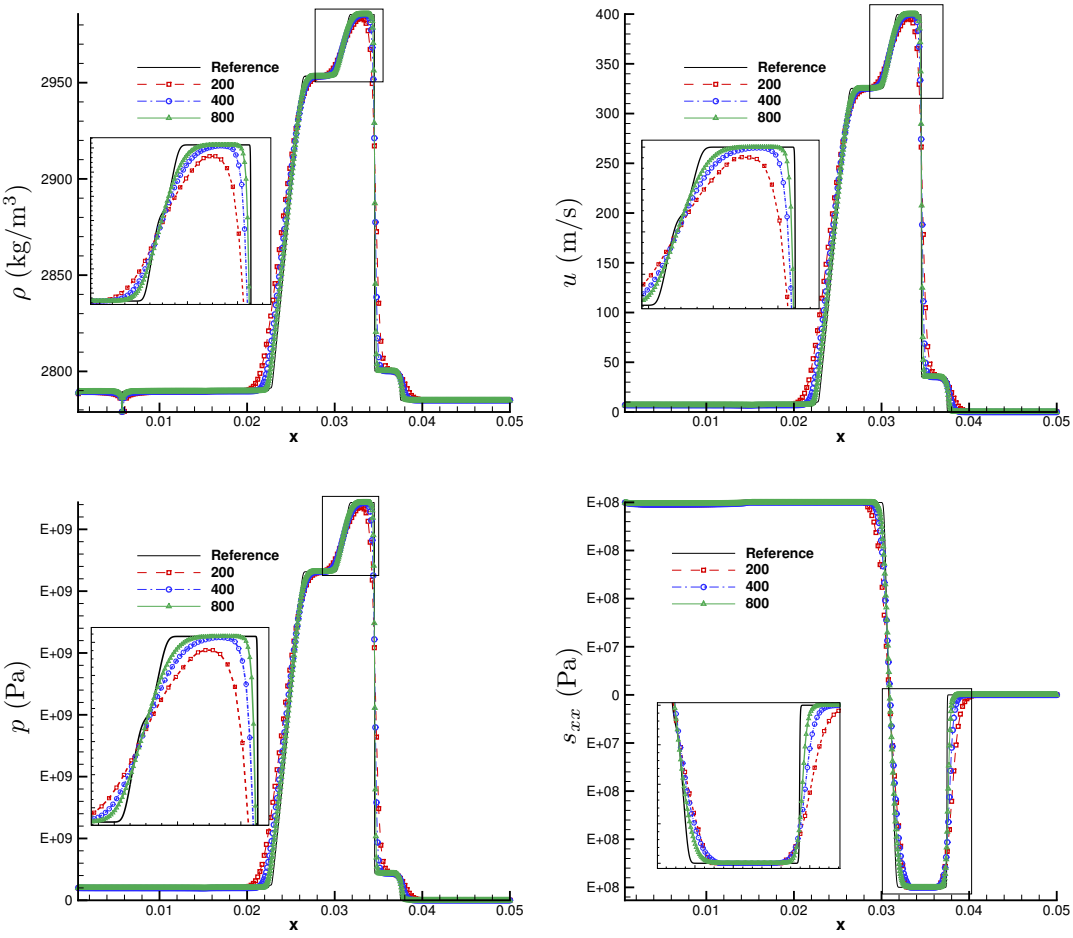

Figure 7: The result of Wilkins problem

The left boundary is set as free boundary and on the right we use a wall boundary condition. The final time is $t = 5 \times 10^{-6}$s. In Fig.7, we give the results simulated with 200, 400 and 800 cells, the reference result is given by the refined mesh with 4000 cells. Showed in the figures and their locally enlarged plots, the elastic and plastic right-going shocks and the reflected elastic and plastic rarefaction waves are well resolved without numerical oscillation.

5.4 Multi-material problem 1

Here we consider the multi-material problem without the plasticity effect. A similar case is used in Ref.([15]). In this test, a moving copper strikes on an aluminium plate. The parameters for the EOS and constitutive model for aluminum and copper are $(\rho_0, a_0, \Gamma_0, s, \mu)_{\text{Al}} = (8930\text{kg/m}^3, 3940\text{m/s}, 2, 1.49, 2.76, 2.76 \times 10^{10}\text{Pa})$ and $(\rho_0, a_0, \Gamma_0, s, \mu)_{\text{copper}} = (2785\text{kg/m}^3, 5328\text{m/s}, 2, 1.338, 4.5 \times 10^{10}\text{Pa})$, respectively. In order to remove the influence of the plasticity effect, we use a very large un-physical yielding strength $Y_0 = 3 \times 10^{12}$Pa. The initial conditions of this problem are

$$\begin{cases} \rho = 2785\text{kg/m}^3, \quad u = u_0, \quad p = 10^{-12}\text{Pa}, s_{xx} = 0, \quad \text{if } \ 0\text{m} \le x \le 2.5 \times 10^{-2}\text{m}, \\ \rho = 8930\text{kg/m}^3, \quad u = 0\text{m/s}, \quad p = 10^{-12}\text{Pa}, s_{xx} = 0, \quad \text{if } \ 2.5 \times 10^{-2}\text{m} \le x \le 50 \times 10^{-2}\text{m}. \end{cases} \tag{5.6}$$

In this case we take $u_0 = 100$m/s. Figure 8 shows the numerical results computed by the scheme with HLLCE and the scheme with MHLLCEP at the final time $t = 2 \times 10^{-6}s$, the reference is given by a refined mesh with

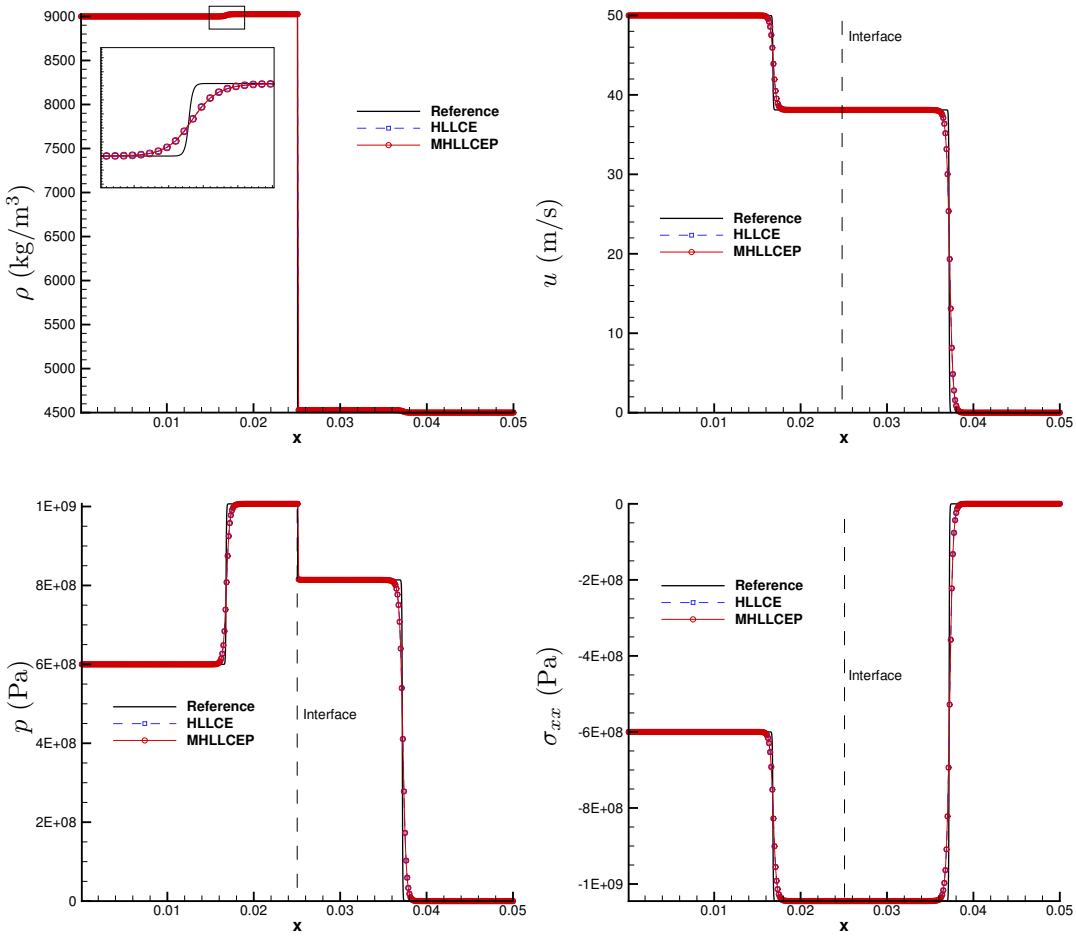

Figure 8: The result of multi-material problem 1

4000 cells. We can see there is little difference between the two schemes for the multi-material case without plastic waves.

5.5 Multi-material problem 2

Next, we consider a similar problem but with plasticity effect. The yield strengths are $Y_0^{\text{Copper}} = 9 \times 10^7$ and $Y_0^{\text{Al}} = 3 \times 10^8$, respectively. All other parameters are same to those in problem 5.4. The initial condition is also as same as Eq.(5.6), we consider this case with a velocity of $u_0 = 60$m/s. Fig.9 gives the results at final time $t = 2 \times 10^{-6}$s with 400 cells, the solution computed by the scheme with HLLCE is taken as a comparison. The reference solution is given by a refine mesh with 4000 cells. We can see that using HLLCE, the Cauchy stress is not continuous across the interface, which does not confirm with the relation of Eq.(3.18), while with MHLLCEP, we can get a correct and stable result.

Conclutions

In this paper, a multi-material HLLC-type approximate Riemann solver with both the elastic and plastic waves (MHLLCEP) is constructed for 1D elastic-plastic flows with a hypo-elastic constitutive model and the von Mises yielding condition. In the construction of MHLLCEP, we do not use any assumption and so describe and evaluate the plastic waves more accurate than that in HLLCE. Based on MHLLCEP, combining

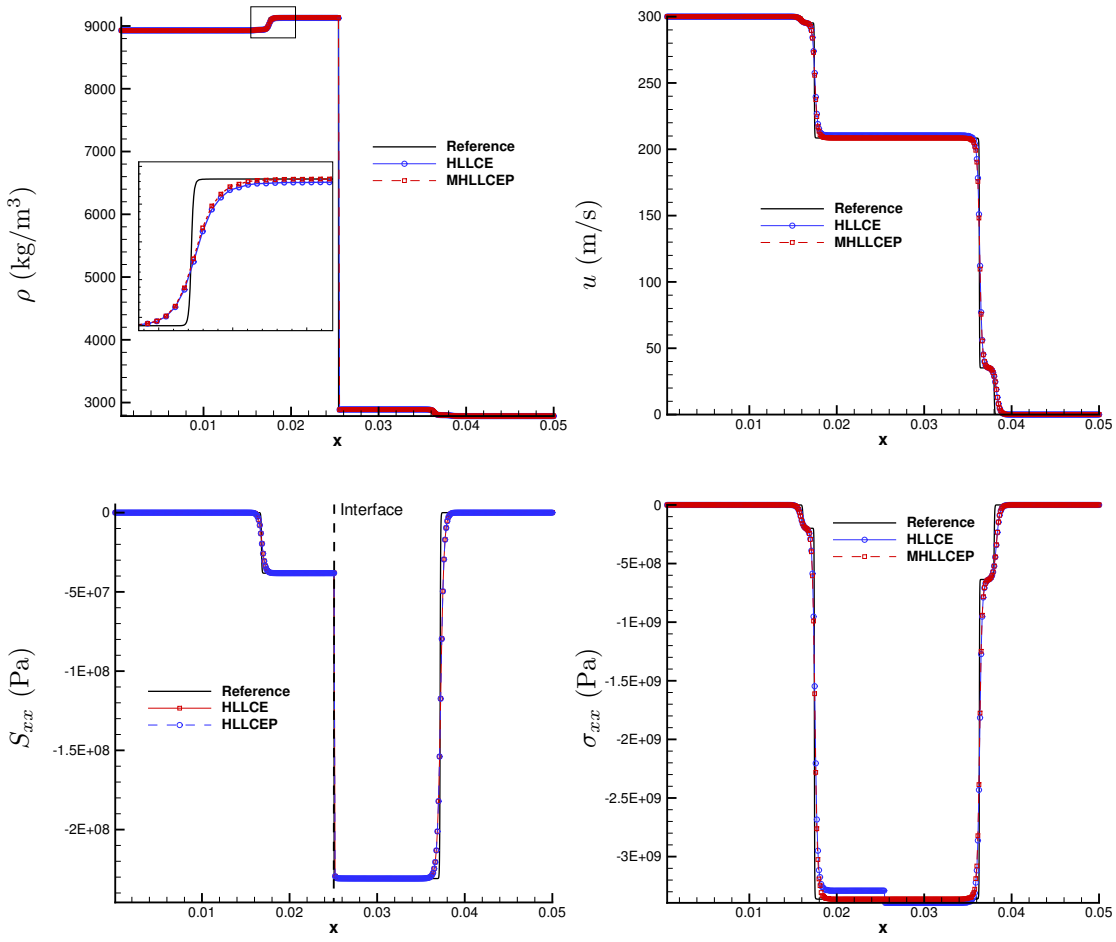

Figure 9: The result of multi-material problem 2

with the ghost cell method near the multi-material interface, a third-order WENO reconstruction method and a third-order TVD-Runge-Kutta method in time, a high-order cell-centered Lagrangian scheme for 1D multi-material elastic flows is built. Verified by the numerical experiments, both the plastic waves and elastic waves can be resolved stably and accurately. Especially in the multi-material elastic-plastic case, the result solved by HLLCE scheme is with large error, but with the new scheme we can get a more reasonable result.

Acknowledgement

This work was supported by NSFC(Grant Nos. 11672047) and Science Challenge Project (Grant No. JCKY2016212A502).

References

[1] M. L. Wilkins, Calculation of elastic-plastic flow, Tech. rep., California Univ Livermore Radiation Lab (1963).

[2] J. A. Trangenstein, P. Colella, A higher-order godunov method for modeling finite deformation in elastic-plastic solids, Communications on Pure and Applied mathematics 44 (1) (1991) 41–100.

[3] G. Miller, P. Colella, A high-order eulerian godunov method for elastic–plastic flow in solids, Journal of computational physics 167 (1) (2001) 131–176.

[4] P. T. Barton, D. Drikakis, E. Romenski, V. A. Titarev, Exact and approximate solutions of riemann problems in non-linear elasticity, Journal of Computational Physics 228 (18) (2009) 7046–7068.

[5] D. Burton, T. Carney, N. Morgan, S. Sambasivan, M. Shashkov, A cell-centered lagrangian godunov-like method for solid dynamics, Computers & Fluids 83 (2013) 33–47.

[6] G. Kluth, B. Després, Discretization of hyperelasticity on unstructured mesh with a cell-centered lagrangian scheme, Journal of Computational Physics 229 (24) (2010) 9092–9118.

[7] P.-H. Maire, R. Abgrall, J. Breil, R. LoubèRe, B. Rebourcet, A nominally second-order cell-centered lagrangian scheme for simulating elastic–plastic flows on two-dimensional unstructured grids, Journal of Computational Physics 235 (2013) 626–665.

[8] J.-B. Cheng, W. Huang, S. Jiang, B. Tian, A third-order moving mesh cell-centered scheme for one-dimensional elastic-plastic flows, Journal of Computational Physics 349 (2017) 137–153.

[9] S. L. Gavrilyuk, N. Favrie, R. Saurel, Modelling wave dynamics of compressible elastic materials, Journal of computational physics 227 (5) (2008) 2941–2969.

[10] B. Despres, A geometrical approach to nonconservative shocks and elastoplastic shocks, Archive for Rational Mechanics and Analysis 186 (2) (2007) 275–308.

[11] J.-B. Cheng, E. F. Toro, S. Jiang, M. Yu, W. Tang, A high-order cell-centered lagrangian scheme for one-dimensional elastic–plastic problems, Computers & Fluids 122 (2015) 136–152.

[12] J. Cheng, Harten-lax-van leer-contact (hllc) approximation riemann solver with elastic waves for one-dimensional elastic-plastic problems, Applied Mathematics and Mechanics 37 (11) (2016) 1517–1538.

[13] S. Liu, Y. Shen, B. Chen, F. Zeng, Novel local smoothness indicators for improving the third-order weno scheme, International Journal for Numerical Methods in Fluids 87 (2) (2018) 51–69.

[14] P.-H. Maire, R. Abgrall, J. Breil, J. Ovadia, A cell-centered lagrangian scheme for two-dimensional compressible flow problems, SIAM Journal on Scientific Computing 29 (4) (2007) 1781–1824.

[15] N. S. Ghaisas, A. Subramaniam, S. K. Lele, High-order eulerian methods for elastic-plastic flow in solids and coupling with fluid flows, in: 46th AIAA Fluid Dynamics Conference, 2016, p. 3350.